

Impact of physical model error on State Estimation for neutronics applications

Y. Conjunco Taumhas, D. Labeurthre, F. Madiot, O. Mula, T. Taddei

Abstract

In this paper, we consider the inverse problem of state estimation of nuclear power fields in a power plant from a limited number of observations of the neutron flux. For this, we use the Parametrized Background Data Weak approach. The method combines the observations with a parametrized PDE model for the behavior of the neutron flux. Since, in general, even the most sophisticated models cannot perfectly capture reality, an inevitable model error is made. We investigate the impact of the model error in the power reconstruction when we use a diffusion model for the neutron flux, and assume that the true physics are governed by a neutron transport model.

Introduction

In the field of nuclear engineering, numerical methods play a crucial role at several stages: they are involved in important assessments and decisions related to design, safety, energy efficiency, and reactor loading plans. In this paper, we focus on the task of providing real time information about the spatial distribution of the nuclear power generated by a nuclear reactor from a limited number of measurement observations. We combine this data with physical models in order to provide a complete spatial reconstruction of the power field. This task is a state estimation problem, and we work with the Parametrized Background Data Weak (PBDW), originally introduced in [1]. The method has the appealing feature of providing very fast reconstructions by leveraging techniques from model order reduction of parametric Partial Differential Equations (PDEs). We refer to [2, 3, 4, 5] for theoretical analysis of the method, optimal recovery results and nonlinear extensions. A recent overview may be found in [6].

The main ideas of the above state estimation methodology have been applied to the field of nuclear physics for applications connected to neutronics (see [7, 8, 9]). We could also cite other works such as [10, 11, 12, 13, 14] which study the forward reduced modeling problem for neutronics (compared to these works, note that there is a salient difference in the nature of the task that we consider, which is inverse state estimation). In this paper, we again consider neutronics but our goal is to study the impact of inaccuracies in the physical model that is

involved in the reconstruction algorithm, and which is often assumed to perfectly describe reality. This assumption goes beyond the present application on neutronics but studying it for this particular topic has the advantage that we have two very well identified models with different levels of accuracy, thereby allowing to examine synthetically what one can expect when working in a real application scenario.

In neutronics, the most accurate physical model is the so-called neutron transport equation which describes the evolution of the neutronic population in a reactor core by expressing it in the form of a balance between produced and lost neutrons [15]. This model is often approximated at the reactor core scale by a neutron diffusion model to save computing time. This is why in this work, we explore the impact of model inaccuracies by applying a reconstruction based on a diffusion model for the neutron flux, and then assuming that the true physical system is governed by a neutron transport model.

The paper is organized as follows. Section 1 is devoted to presenting inverse state estimation problems and the PBDW method. Section 2 details the application of the methodology to the reconstruction of nuclear power. Section 3 provides some numerical results.

1 Inverse State Estimation with PBDW

In this section, we introduce the problem of state estimation, and the Parametrized Background Data Weak method which combines measurement observations and reduced models from parametric PDEs. We refer the reader to [6] for an overview of inverse problem algorithms using these elements.

Let \mathcal{R} be a fixed given domain of \mathbb{R}^d with dimension $d \geq 1$, and let V be a Hilbert space defined over \mathcal{R} . In our application, \mathcal{R} will be defined as the nuclear reactor domain. The space is endowed with an inner product $\langle \cdot, \cdot \rangle$ and induced norm $\|\cdot\|$. The choice of V must be relevant for the problem under consideration: typical options are L^2 , H^1 ; for pointwise measurements, a Reproducing Kernel Hilbert Space should be considered.

Our goal is to recover an unknown function $u \in V$ from m measurement observations

$$y_i = \ell_i(u), \quad i = 1, \dots, m, \quad (1)$$

where the ℓ_i are linearly independent linear forms from the dual V' . Note that we have assumed that experimental observations are perfect; however, the methodology could be extended to deal with noisy measurements (see, e.g., [16, 17, 18]). In practical applications, each ℓ_i models a sensor device which is used to collect the measurement data $\ell_i(u)$. In the applications that we present in our numerical tests, the observations come from sensors for the neutron flux which are placed in the reactor.

We denote by $\omega_i \in V$ the Riesz representers of the ℓ_i . They are defined via the variational equation

$$\langle \omega_i, v \rangle = \ell_i(v), \quad \forall v \in V.$$

Since the ℓ_i are linearly independent in V' , so are the ω_i in V and they span an m -dimensional space

$$W_m = \text{span}\{\omega_1, \dots, \omega_m\} \subset V.$$

When there is no measurement noise, knowing the observations $y_i = \ell_i(u)$ is equivalent to knowing the orthogonal projection

$$\omega = P_{W_m} u. \quad (2)$$

In this setting, the task of recovering u from the measurement observation ω can be viewed as building a recovery algorithm

$$A : W_m \mapsto V$$

such that $A(P_{W_m} u)$ is a good approximation of u in the sense that $\|u - A(P_{W_m} u)\|$ is small.

Recovering u from the measurements $P_{W_m} u$ is a very ill-posed problem since V is generally a space of very high or infinite dimension so, in general, there are infinitely many $v \in V$ such that $P_{W_m} v = \omega$. It is thus necessary to add some a priori information on u in order to recover the state up to a guaranteed accuracy. In the following, we work in the setting where u is a solution to some parameter-dependent PDE of the general form

$$\mathcal{P}(u, \mu) = 0,$$

where \mathcal{P} is a differential operator and μ is a vector of parameters that describe some physical property and belong to a given set $\mathcal{D} \subset \mathbb{R}^p$. For every $\mu \in \mathcal{D}$, we assume that the PDE has a unique solution $u = u(\mu) \in V$. Therefore, our prior on u is that it belongs to the so-called *solution manifold*

$$\mathcal{M} := \{u(\mu) \in V : \mu \in \mathcal{D}\}. \quad (3)$$

In practical applications, the PDE model \mathcal{P} might not be known exactly or might be too expensive to evaluate: we should thus rely on a surrogate approximate model to perform state estimation.

Performance Benchmarks: The quality of a recovery mapping A is quantified in two ways:

- If the sole prior information is that u belongs to the manifold \mathcal{M} , the performance is usually measured by the worst case reconstruction error

$$E_{\text{wc}}(A, \mathcal{M}) = \sup_{u \in \mathcal{M}} \|u - A(P_{W_m} u)\|. \quad (4)$$

- In some cases u is described by a probability distribution p on V supported on \mathcal{M} . This distribution is itself induced by a probability distribution on \mathcal{D} that is assumed to be known. When no information about the distribution is available, usually the uniform distribution is taken. In this Bayesian-type setting, the performance is usually measured in an average sense through the mean-square error

$$E_{\text{ms}}^2(A, \mathcal{M}) = \mathbb{E} (\|u - A(P_{W_m} u)\|^2) = \int_V \|u - A(P_{W_m} u)\|^2 dp(u), \quad (5)$$

and it naturally follows that $E_{\text{ms}}(A, \mathcal{M}) \leq E_{\text{wc}}(A, \mathcal{M})$.

PBDW algorithm: In this work, we resort to the Parametrized-Background Data-Weak algorithm (PBDW, [1]) to estimate the state u . Other choices would of course be possible but the PBDW algorithm is relevant for the following reasons:

- **Simplicity and Speed:** It is easily implementable and it provides reconstructions in near-real time.
- **Optimality:** It has strong connections with optimal linear reconstruction algorithms as has been studied in [19, 4].
- **Extensions:** If required, the algorithm can easily be extended to enhance its reconstruction performance (see [5, 20]). In particular, it is shown in [5] that piecewise PBDW reconstruction strategy can deliver near-optimal performance. The PBDW algorithm can also be easily adapted to accommodate noisy measurements (see [16, 17]) and some easy-to-implement extension to mitigate the model error exist (in the following however, we assume the PDE model is perfect for the sake of simplicity).

Since the geometry of \mathcal{M} is generally complex, optimization tasks posed on \mathcal{M} are difficult (lack of convexity, high evaluation costs for different parameters). Therefore, instead of working with \mathcal{M} , PBDW works with a linear (or affine) space V_n of reduced dimension n which is expected to approximate the solution manifold well in the sense that the approximation error of the manifold

$$\delta_n^{(\text{wc})} := \sup_{u \in \mathcal{M}} \text{dist}(u, V_n), \quad \text{or} \quad \delta_n^{(\text{ms})} := \mathbb{E} (\text{dist}(u, V_n)^2)^{1/2} \quad (6)$$

decays rapidly if we increase the dimension n . It has been proven in [21] that it is possible to find such hierarchies of spaces $(V_n)_{n \geq 1}$ for certain manifolds coming from classes of elliptic and parabolic problems, and numerous strategies have been proposed to build the spaces in practice (see, e.g., [22, 23] for reduced basis techniques and [21, 24] for polynomial approximations in the μ variable).

Assuming that we are given a reduced model V_n with $1 \leq n \leq m$, the PBDW algorithm

$$A_{m,n}^{(\text{pbdw})} : W_m \rightarrow V$$

gives for any $\omega \in W_m$ a solution of

$$A_{m,n}^{(\text{pbdw})}(\omega) \in \arg \min_{u \in \omega + W(\mathcal{R})^\perp} \text{dist}(u, V_n). \quad (7)$$

The minimizer is unique as soon as $n \leq m$ and $\beta(V_n, W_m) > 0$, which is an assumption to which we adhere in the following. The quantity β is defined as follows. For any pair of closed subspaces (E, F) of V , $\beta(E, F)$ is defined as

$$\beta(E, F) := \inf_{e \in E} \sup_{f \in F} \frac{\langle e, f \rangle}{\|e\| \|f\|} = \inf_{e \in E} \frac{\|P_F e\|}{\|e\|} \in [0, 1]. \quad (8)$$

We can prove that $A_{m,n}^{(\text{pbdw})}$ is a bounded linear map from W_m to $V_n \oplus (W_m \cap V_n^\perp)$.

In practice, solving problem (7) boils down to solving a linear least squares minimization problem whose cost is essentially of order $n^2 + m$, and we can compute $\beta(V_n, W_m)$ by finding the smallest eigenvalue of an $n \times n$ matrix. We refer, e.g., to [6, Appendix A, B] for details on how to compute these elements in practice. It follows that, since in general m is not very large, if the dimension n of the reduced model is moderate, the reconstruction with (7) can take place in close to real-time.

For any $u \in V$, the reconstruction error is bounded by

$$\|u - A_{m,n}^{(\text{pbdw})}(\omega)\| \leq \beta^{-1}(V_n, W_m) \|u - P_{V_n \oplus (W_m \cap V_n^\perp)} u\| \leq \beta^{-1}(V_n, W_m) \|u - P_{V_n} u\|, \quad (9)$$

where we have omitted the dependency of the spaces on \mathcal{R} in order not to overload the notation, and we will keep omitting this dependency until the end of this section. Depending on whether V_n is built to address the worst case or mean square error, the reconstruction performance over the whole manifold \mathcal{M} is bounded by

$$e_{m,n}^{(\text{wc, pbdw})} := E_{\text{wc}}(A_{m,n}^{(\text{pbdw})}, \mathcal{M}) \leq \beta^{-1}(V_n, W_m) \max_{u \in \mathcal{M}} \text{dist}(u, V_n \oplus (V_n^\perp \cap W_m)) \leq \beta^{-1}(V_n, W_m) \delta_n^{(\text{wc})}, \quad (10)$$

or

$$\begin{aligned} e_{m,n}^{(\text{ms, pbdw})} &:= E_{\text{ms}}(A_{m,n}^{(\text{pbdw})}, \mathcal{M}) \leq \beta^{-1}(V_n, W_m) \mathbb{E} \left(\text{dist}(u, V_n \oplus (V_n^\perp \cap W_m))^2 \right)^{1/2} \\ &\leq \beta^{-1}(V_n, W_m) \delta_n^{(\text{ms})}. \end{aligned} \quad (11)$$

Note that $\beta(V_n, W_m)$ can be understood as a stability constant. It can also be interpreted as the cosine of the angle between V_n and W_m . The error bounds involve the distance of u to the space $V_n \oplus (V_n^\perp \cap W_m)$ which provides slightly more accuracy than the reduced model V_n alone. This term is the reason why it is sometimes said that the method can correct model error to some extent. In the following, to ease the reading we will write errors only with the second type of bounds (11) that do not involve the correction part on $V_n^\perp \cap W_m$.

An important observation is that for a fixed measurement space W_m (which is the setting in our numerical tests), the error functions

$$n \mapsto e_{m,n}^{(\text{wc, pbdw})}, \quad \text{and} \quad n \mapsto e_{m,n}^{(\text{ms, pbdw})}$$

reach a minimal value for a certain dimension n_{wc}^* and n_{ms}^* as the dimension n varies from 1 to m . This behavior is due to the trade-off between:

- the improvement of the approximation properties of V_n as n grows ($\delta_n^{(\text{wc})}$ and $\delta_n^{(\text{ms})} \rightarrow 0$ as n grows)
- the degradation of the stability of the algorithm, given here by the decrease of $\beta(V_n, W_m)$ to 0 as $n \rightarrow m$. When $n > m$, $\beta(V_n, W_m) = 0$.

As a result, the best reconstruction performance with PBDW is given by

$$e_{m,n_{\text{wc}}^*}^{(\text{wc, pbdw})} = \min_{1 \leq n \leq m} e_{m,n}^{(\text{wc, pbdw})}, \quad \text{or} \quad e_{m,n_{\text{ms}}^*}^{(\text{ms, pbdw})} = \min_{1 \leq n \leq m} e_{m,n}^{(\text{ms, pbdw})}.$$

Noise and Model Error: To account for measurement noise and model bias in the above analysis, let us assume that we get noisy observations $\tilde{\omega} = \omega + \eta$ with $\|\eta\| \leq \varepsilon_{noise}$. Suppose also that the true state u does not lie in \mathcal{M} but satisfies $\text{dist}(u, \mathcal{M}) \leq \varepsilon_{model}$. We can prove that the error bound (9) should be modified into

$$\|u - A_{m,n}^{(\text{pbdw})}(\tilde{\omega})\| \leq \beta^{-1}(V_n, W_m)(\|u - P_{V_n}u\| + \varepsilon_{noise} + \varepsilon_{model}).$$

Thus (10) and (11) become

$$e_{m,n}^{(\text{wc, pbdw})} := E_{\text{wc}}(A_{m,n}^{(\text{pbdw})}, \mathcal{M}) \leq \beta^{-1}(V_n, W_m)(\delta_n^{(\text{wc})} + \varepsilon_{noise} + \varepsilon_{model}), \quad (12)$$

and

$$e_{m,n}^{(\text{ms, pbdw})} := E_{\text{ms}}(A_{m,n}^{(\text{pbdw})}, \mathcal{M}) \leq \beta^{-1}(V_n, W_m)(\delta_n^{(\text{ms})} + \varepsilon_{noise} + \varepsilon_{model}). \quad (13)$$

Note that the estimation accuracy benefits from decreasing the model error, and the noise. Since both errors have the same additive effect on the reconstruction accuracy, model error could be understood as measurement error and vice-versa. However, since the underlying physical reasons leading to model and measurement error are entirely different, it is preferable to clearly keep both concepts separately. Note further that the computational complexity of the method is not affected by these errors. This is in contrast to Bayesian methods for which small noise levels induce computational difficulties due to the concentration of the posterior distribution.

Sensor modeling error: Another error that can occur comes from our choice of the observation functions ω_i which are built to mimic the response of the sensor devices. Suppose that we work with imperfect functions $\tilde{\omega}_i$ that deviate from the exact one ω_i with $\|\omega_i - \tilde{\omega}_i\| \leq \rho$ for some $\rho > 0$. Then noiseless observations can be written as

$$y_i = \ell_i(u) = \langle \omega_i, u \rangle = \langle \tilde{\omega}_i, u \rangle + \langle \omega_i - \tilde{\omega}_i, u \rangle.$$

The right hand side tells us that by working with the inexact $\tilde{\omega}_i$, we are introducing a term of noise which is $\langle \omega_i - \tilde{\omega}_i, u \rangle$. The noise has level $\rho\|u\|$. It follows that working with an inexact representation of the sensor response can be understood as introducing additional noise to the observations.

2 Application to the reconstruction of nuclear power

In this work, we apply the above general framework to reconstruct the nuclear power P generated in a nuclear reactor core defined on a convex domain \mathcal{R} . The power P is a real-valued function in \mathcal{R} , $P : \mathcal{R} \rightarrow \mathbb{R}_+$, and in the following we reconstruct it by viewing it as a function in the space

$$V = L^2(\mathcal{R}).$$

The nuclear power P we want to rebuild always comes from the neutron transport model. However, the spaces used to reconstruct P will be divided in two cases. One space is made up of solutions of the transport model while the other is made up of solutions of the diffusion model as discussed in the following sections.

2.1 The neutron transport model

We assume that the reactor is in a stationary state where the neutron population ψ , usually called the angular flux, depends on (r, ω, E) , namely the spatial position $r \in \mathcal{R} \subset \mathbb{R}^d$, the direction of propagation $\omega \in \mathbb{S}_d$ where \mathbb{S}_d is the unit sphere of \mathbb{R}^d , and the kinetic energy $E \in \mathbb{R}^+$. We work with a multi-group approach where we consider a discrete set of energies $E_G < \dots < E_0$, and we denote

$$\psi(r, \omega, [E_g, E_{g-1}]) := \psi^g(r, \omega), \quad \forall (r, \omega) \in \mathcal{R} \times \mathbb{S}_d, \quad \forall g \in \{1, \dots, G\}.$$

With this notation, the neutron transport equation is a generalized eigenvalue problem in which we search for a multigroup flux $\psi = (\psi^g)_{g=1}^G$, and a generalized eigenvalue $\lambda \in \mathbb{C}^*$ (see [25])

$$\begin{cases} L^g \psi^g(r, \omega) = H^g \psi(r, \omega) + \lambda F^g \psi^g(r, \omega) & \text{in } \mathcal{R} \times \mathbb{S}_2, \quad \forall g \in \{1, \dots, G\} \\ \psi(r, \omega) = 0 & \text{on } \partial\Gamma_- := \{(r, \omega) \in \partial\mathcal{R} \times \mathbb{S}_d : n(r) \cdot \omega < 0\}, \end{cases} \quad (14)$$

where

$L^g \psi^g(r, \omega) := (\omega \cdot \nabla + \Sigma_t^g(r)) \psi^g(r, \omega)$ is the advection operator,

$H^g \psi(r, \omega) := \sum_{g'=1}^G \int_{\mathbb{S}_2} \Sigma_s^{g' \rightarrow g}(r, \omega' \cdot \omega) \psi^{g'}(r, \omega') d\omega'$ is the scattering operator,

$F^g \psi(r, \omega) := \frac{\chi^g(r)}{4\pi} \sum_{g'=1}^G (\nu \Sigma_f)^{g'}(r) \int_{\mathbb{S}_2} \psi^{g'}(r, \omega) d\omega$ is the fission operator.

In the listed terms, $\Sigma_t^g(r)$ denotes the total cross-section and $\Sigma_s^{g' \rightarrow g}(r, \omega' \cdot \omega)$ is the scattering cross-section from energy group g' and direction ω' to energy group g and direction ω , $\Sigma_f^g(r)$ is the fission cross-section, $\nu^g(r)$ is the average number of neutrons emitted per fission and $\chi^g(r)$ is the fission spectrum. We suppose that all the coefficients are measurable bounded functions of their arguments.

Under certain conditions (which we assume to be satisfied in the following), the eigenvalue λ_{\min} with the smallest modulus is simple, real and strictly positive. We refer to [26, Theorem 2.2] for the sketch of the proof detailed in [27, Theorem 2.1.1, p 92]. The associated eigenfunction

ψ belongs to the Hilbert space $W^2(\mathcal{R})^G$ where $W^2(\mathcal{R} \times \mathbb{S}_2) = \{\psi \in L^2(\mathcal{R} \times \mathbb{S}_2) \text{ s.t. } \omega \cdot \nabla \psi \in L^2(\mathcal{R} \times \mathbb{S}_2)\}$, is also real and positive at almost every $(x, \omega) \in \mathcal{R} \times \mathbb{S}_2$. With this model, once the neutron flux is computed by solving (14) numerically, the nuclear power is given by

$$P(r) := \sum_{g'=1}^G (\kappa \Sigma_f)^{g'} \int_{\mathbb{S}_2} \psi^{g'}(r, \omega) d\omega, \quad \forall r \in \mathcal{R} \text{ a.e.},$$

where $\kappa^g \in L^\infty(\mathcal{R})$ is the released energy per fission and since $\psi \in (W^2(\mathcal{R} \times \mathbb{S}_2))^G$, we have that $P \in V$.

2.2 The neutron diffusion equations

In this work, the neutron flux ϕ is modeled with the two-group neutron diffusion equation with null flux boundary conditions. So ϕ has two energy groups $\phi = (\phi^1, \phi^2)$. Index 1 denotes the high energy group and 2 the thermal energy one. The flux is the solution to the following eigenvalue problem (see [15])

Find $(\lambda, \phi) \in \mathbb{C} \times (H^1(\mathcal{R}) \times H^1(\mathcal{R}))$ such that for all $x \in \mathcal{R}$,

$$\begin{cases} -\nabla(D^1(r)\nabla\phi^1(r)) + \Sigma_a^1(r)\phi^1(r) - \Sigma_{s,0}^{2 \rightarrow 1}(r)\phi^2(r) = \lambda(\chi^1(r)(\nu\Sigma_f)^1(r)\phi^1 + \chi^1(r)(\nu\Sigma_f)^2(r)\phi^2(r)) \\ -\nabla(D^2(r)\nabla\phi^2(r)) + \Sigma_a^2(r)\phi^2(r) - \Sigma_{s,0}^{1 \rightarrow 2}(r)\phi^1(r) = \lambda(\chi^2(r)(\nu\Sigma_f)^1(r)\phi^1(r) + \chi^2(r)(\nu\Sigma_f)^2(r)\phi^2(r)), \end{cases} \quad (15)$$

with

$$D^g(r)\nabla\phi^g(r) \cdot n + \frac{1}{2}\phi^g(r) = 0 \quad \text{on } \partial\mathcal{R}, \text{ for } g = 1, 2.$$

The coefficients involved are the following:

- $D^g(r)$ is the diffusion coefficient of group g with $g \in \{1, 2\}$.
- $\Sigma_a^g(r)$ is the macroscopic absorption cross section of group g .
- $\Sigma_{s,0}^{g' \rightarrow g}(r)$ is the macroscopic scattering cross section of anisotropy order 0 from group g' to g .
- $\chi^g(r)$ is the fission spectrum of group g .

We assume that they are either constant or piecewise constant in \mathcal{R} so we can view them as functions from $L^\infty(\mathcal{R})$.

The generated power is

$$P := (\kappa \Sigma_f)^1 \phi^1 + (\kappa \Sigma_f)^2 \phi^2, \quad (16)$$

and since ϕ^1 and $\phi^2 \in H^1(\mathcal{R})$, we have $P \in V$.

We next make some comments on the coefficients and recall well-posedness results of the eigenvalue problem (15). First of all, the first four coefficients (D^g , Σ_a^g , $\Sigma_{s,0}^{1 \rightarrow 2}$, $\Sigma_{s,0}^{2 \rightarrow 1}$ and $(\nu\Sigma_f)^g$) might depend on the spatial variable. In the following, we assume that they are either constant or piecewise constant so that our set of parameters is

$$\mu = \{D^1, D^2, \Sigma_a^1, \Sigma_a^2, \Sigma_{s,0}^{1 \rightarrow 2}, (\nu\Sigma_f)^1, (\nu\Sigma_f)^2, \chi^1, \chi^2\}. \quad (17)$$

By abuse of notation, in (17) we have written D^g to denote the set of values that this coefficient might take in space and similarly for the other parameters.

Under some mild conditions on the parameters μ , the eigenvalue λ_{\min} with the smallest modulus is simple, real and strictly positive (see [25, Chapter XXI]). The associated eigenfunction ϕ is also real and positive at almost every point $x \in \mathcal{R}$ and it is what is classically called the flux. In neutronics, it is customary to work with the inverse of λ_{\min} , which is called the multiplication factor

$$k_{\text{eff}} := 1/\lambda_{\min}. \quad (18)$$

Therefore k_{eff} is not a parameter in our setting because, for each value of the parameters μ , k_{eff} is determined by the solution to the eigenvalue problem.

If the parameters of our diffusion model range in, say,

$$D^1 \in [D_{\min}^1, D_{\max}^1], \quad D^2 \in [D_{\min}^2, D_{\max}^2], \dots, \quad \chi^2 \in [\chi_{\min}^2, \chi_{\max}^2],$$

then

$$\mathcal{D} := [D_{\min}^1, D_{\max}^1] \times \dots \times [\chi_{\min}^2, \chi_{\max}^2], \quad (19)$$

and the set of all possible states of the power is given by

$$\mathcal{M}_{\text{diff}} = \{P(\mu) : \mu \in \mathcal{D}\} \subset V, \quad (20)$$

which is the manifold of solutions of our problem.

3 Numerical Examples

3.1 Description of the test case and the numerical solver

The test-case: We consider Model 1 Case 1 of the well-known Takeda neutronics benchmark [28] to build our test case. The geometry of the core is three-dimensional and the domain is $\{(x, y, z) \in \mathbb{R}^3, 0 \leq x \leq 25 \text{ cm}; 0 \leq y \leq 25 \text{ cm}; 0 \leq z \leq 25 \text{ cm}\}$. This test is defined with $G = 2$ energy groups and isotropic scattering and we set $\kappa^g = 1 \text{ MeV}$ for $g = 1, 2$. The reactor core geometry is depicted in Figure 1. In the following, we implicitly refer to the cross-sections and the other coefficients of this test case. Our goal is to reconstruct in real time the spatial

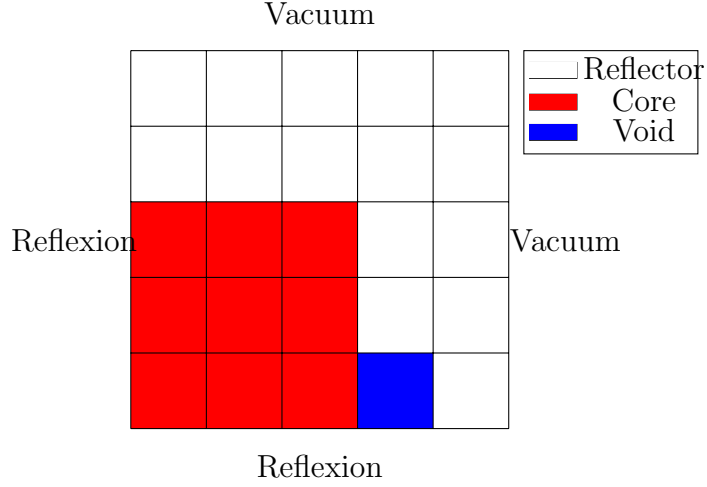


Figure 1: Cross-sectional view of the core ($z = 0$ cm).

power field of the reactor. We assume that the neutron transport equation perfectly describes reality, and the set of all possible states is given by the manifold

$$\mathcal{M}_{\text{tr}} = \{P^{\text{tr}}(\mu) : \mu \in \mathcal{D}\} \subset V.$$

The set of solutions of the neutron diffusion equation is

$$\mathcal{M}_{\text{diff}} = \{P^{\text{diff}}(\mu) : \mu \in \mathcal{D}\} \subset V.$$

It is an imperfect description of the true states given by \mathcal{M}_{tr} .

The parameter set μ from equation (17) is generated by the mapping

$$\begin{aligned} \mu &: [0.8, 1]^5 \subset \mathbb{R}^5 \rightarrow \mathbb{R}^9 \\ \alpha &\mapsto \mu(\alpha) \left(\frac{D^1}{\alpha_1}, \frac{D^2}{\alpha_2}, \alpha_1 \Sigma_a^1, \alpha_2 \Sigma_a^2, \alpha_3 \Sigma_{s,0}^{1 \rightarrow 2}, \alpha_4 (\nu \Sigma_f)^1, \alpha_5 (\nu \Sigma_f)^2, \chi^1, \chi^2 \right). \end{aligned}$$

We can thus view the parameter set either as the 5 dimensional tensorized subset $[0.8, 1]^5$ where α ranges, or as a 5-dimensional surface manifold from \mathbb{R}^9 where the 9 coefficients μ of the neutronic model live.

We work with $m = 54$ measurements observations domains that are placed uniformly in the reactor. They are defined as local averages over small subdomains $\mathcal{R}_i \subset \mathcal{R}$

$$\omega_i(x) = \frac{1}{|\mathcal{R}_i|} \mathbf{1}_{\mathcal{R}_i}(x), \quad \forall x \in \mathcal{R}, i = 1, \dots, m. \quad (21)$$

We compare two cases:

1. **Perfect physical model:** We apply PBDW using reduced models from the transport manifold which represents the true reality in our experiments.
2. **Imperfect physical model:** We assume that a perfect model is out of reach and we use the diffusion manifold. The reconstruction will thus be affected by a model bias.

The solver: To generate the snapshots and the reduced models, we have worked with MINARET [29], a deterministic solver for reactor physics calculations developed in the framework of the APOLLO3[®] code [30]. MINARET can solve either the multigroup neutron transport or diffusion problem from Equations (14) and (15). The numerical scheme to compute the multiplication factor k_{eff} is based on the inverse power method (see, e.g., [15]). MINARET uses the S_N discrete ordinate method to deal with the angular variable, and Discontinuous Galerkin Finite Elements to solve spatially the neutron transport equation [31]. It applies the Symmetric Interior Penalty Galerkin method (SIPG) [32, Chapter 4] for the discretization of the neutron diffusion equation (15). In all cases, the solver uses cylindrical meshes devised by extrusion of a 2D triangular mesh. For our simulations, we work with a level-symmetric formula of order $N = 8$ for the S_N quadrature, and the spatial approximation uses discontinuous \mathbb{P}_1 finite elements of a uniform mesh. The physical output power map is post-processed on an approximation space of dimension $N_h = 540$ (N_h degrees of freedom).

3.2 Case 1: Reconstruction with a perfect physical model

Here we assume that we have access to a perfect description of the physics, and we work with the neutron transport manifold \mathcal{M}_{tr} .

In order to create a reduced space V_n of small dimension $n \ll N_h$, we apply a Proper Orthogonal Decomposition (POD) based on the training set

$$\mathcal{P}_{\text{training}} = \{P^{\text{tr}}(\mu(\alpha)), \alpha \in \{0.8, 0.9, 1\}^5\} \subset \mathcal{M}_{\text{tr}}$$

of power maps obtained from solutions of the transport neutron equations, also called snapshots.

We measure the relative approximation error $\tilde{\delta}_n^{(\text{wc})}$ as defined in Equation (6). For this, we define a collection of power maps of reference

$$\mathcal{P}_{\text{test}} = \{P^{\text{tr}}(\mu(\alpha)), \alpha \in \{0.85, 0.95\}^5\}. \quad (22)$$

Figure 2 shows that the training space is well approximated with a few POD modes. For $n \geq 30$, the relative error between one power map and its projection onto V_n is smaller than 10^{-6} .

We next study the ability to reconstruct the power field with measurement observations, and the PBDW method, as Figure 3 shows in the 3D space. For this, we compute for $1 \leq n \leq m$:

- The relative reconstruction error given by $\tilde{e}_{m,n}^{(\text{wc}, \text{pbdw})} = \max_{u \in \tilde{\mathcal{M}}_{\text{tr}}} \frac{\|u - A_{m,n}^{(\text{pbdw})}(\omega)\|}{\|u\|}$,

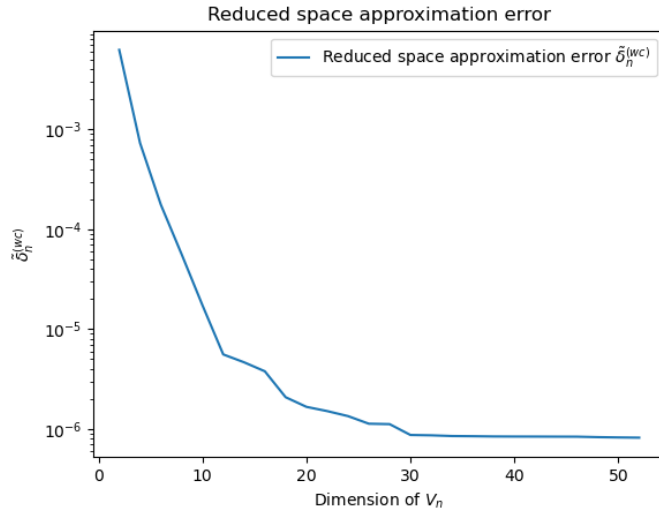


Figure 2: Relative approximation error $\tilde{\delta}_n^{(wc)}$ of the transport manifold \mathcal{M}_{tr} with respect to the dimension n of the reduced space. Here the reduced space is a POD computed using the same manifold \mathcal{M}_{tr} .

- The upper bound of the reconstruction error given by $\beta^{-1}(V_n, W_m)\tilde{\delta}_n^{(wc)}$, as given in Equation (11).

Figure 4 shows that the upper bound is about two orders of magnitude above the actual reconstruction error. This gap is expected to decrease if we use more functions in the test set. The second observation is that the reconstruction accuracy reaches a minimum for a dimension $n^* \approx 25$. If we work with the optimal dimension n^* , an important result is that we can recover the power field from measurement observations at almost the same accuracy ($\approx 10^{-6}$, see Figure 2) as the one given by the orthogonal projection onto V_n (to see this, compare the errors at n^* in Figures 2 and 4).

The behavior of the reconstruction error with the dimension n is connected to a loss of stability illustrated in Figure 5. It warns about a compromise to find between the approximation error of the manifold and the stability in order to optimize the accuracy of the power map reconstruction. One strategy to mitigate stability problems is to find locations for the sensor measurements that span spaces W_m maximizing the value of $\beta(V_n, W_m)$ (see, e.g., [33]).

3.3 Case 2: Reconstruction of the power map from diffusion snapshots

We now consider the diffusion neutron equations as the best available model while the true states are given by the neutron transport model. They are therefore members of \mathcal{M}_{tr} .

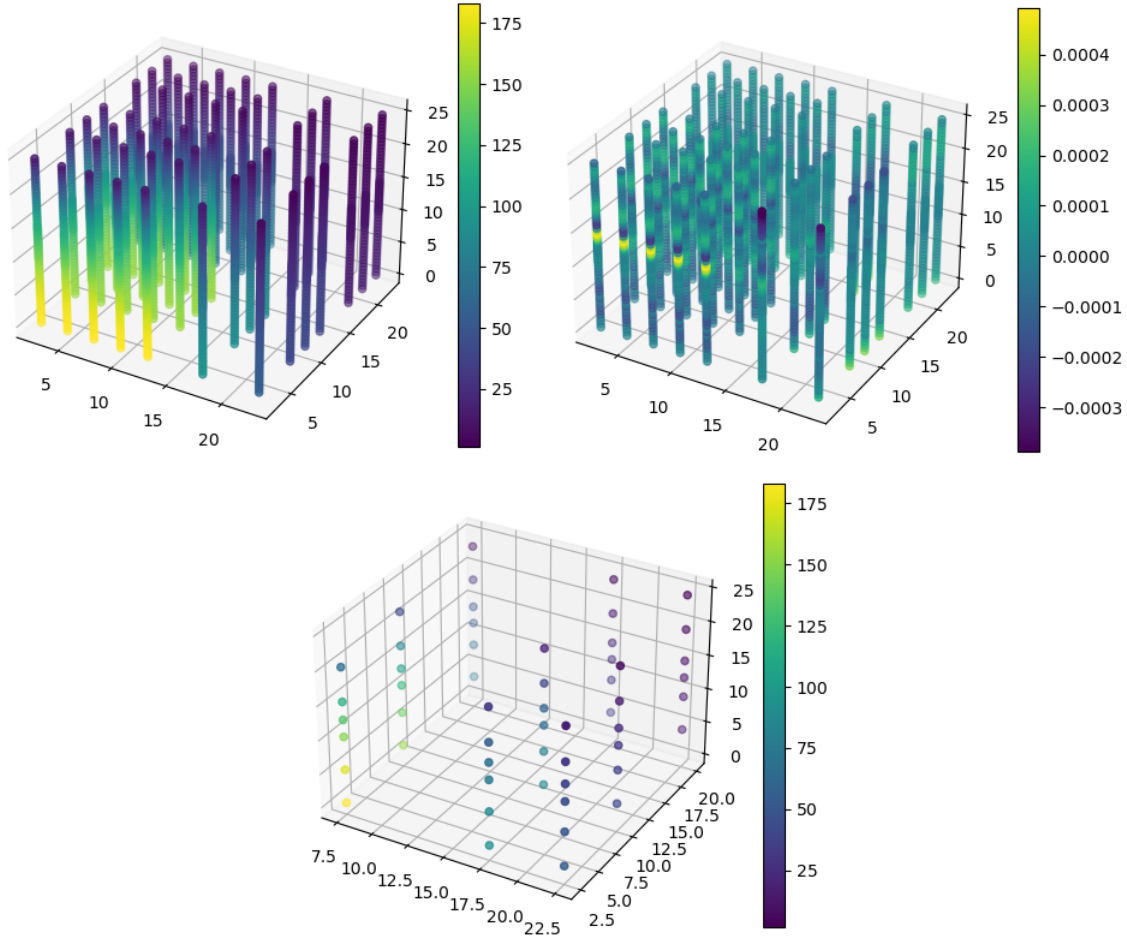


Figure 3: 3D representation of the power map $P^{\text{tr}}(\mu(\alpha))$ with $\alpha = \{0.85\}^5$ (upper left), the algebraic reconstruction error by PBDW (upper right) and the $m = 54$ measurements

Similarly as done in Section 3.2, we apply a POD over a collection

$$\mathcal{P}_{\text{training}} = \{P^{\text{diff}}(\mu(\alpha)) : \alpha \in \{0.8, 0.9, 1\}^5\} \subset \mathcal{M}_{\text{diff}},$$

to create a reduced space V_n of dimension $n \ll N_h$. The main difference lies in the fact that the snapshots are obtained from the neutron diffusion equations, as we consider that the transport model cannot be computed in this section.

Figure 6 shows that the approximation error of the transport manifold \mathcal{M}_{tr} is less accurate than in the previous case due to the bias between the two models. Typically, for $n = 50$, we approximate the manifold at the accuracy of 6×10^{-3} , whereas the approximation with the transport model was about 10^3 times better (compare Figure 6 and Figure 4). Therefore, the reconstruction error will have a similar order of magnitude to those observed for the

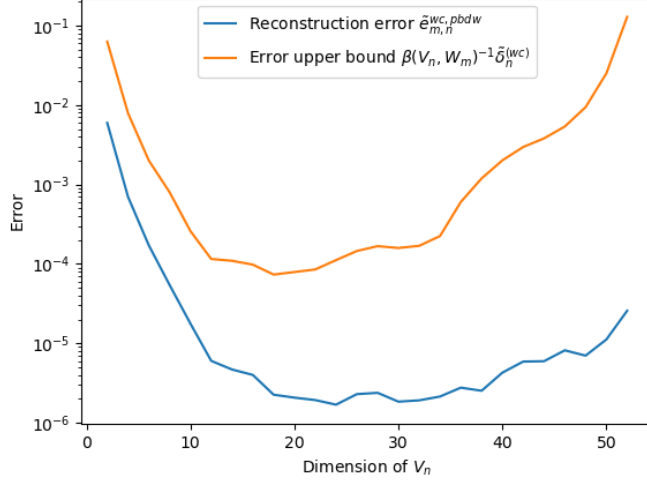


Figure 4: Relative reconstruction error $\tilde{e}_{m,n}^{(\text{wc}, \text{pbdw})}$ (in blue) and error estimate $\beta(V_n, W_m)^{-1} \tilde{\delta}_n^{(\text{wc})}$ (in yellow) with respect to the dimension n of the reduced space

approximation error.

Similarly, we compute for $1 \leq n \leq m$:

- The relative reconstruction error given by $\tilde{e}_{m,n}^{(\text{wc}, \text{pbdw})} = \max_{u \in \tilde{\mathcal{M}}_{\text{tr}}} \frac{\|u - A_{m,n}^{(\text{pbdw})}(\omega)\|}{\|u\|}$,
- The upper bound of the reconstruction error given by $\beta^{-1}(V_n, W_m) \tilde{\delta}_n^{(\text{wc})}$, as given in Equation (11).

As done before, the PBDW reconstruction procedure is then performed by extracting measurements over the collection power maps of reference defined in (22). Figure 7 illustrates that the minimum for the reconstruction error reaches about 1.5×10^{-2} for $n^* \approx 35$. The gap between the reconstruction error and its estimate here is bigger as the stability plays a secondary role. Hence, the reconstruction error is only led by the model bias.

Figures 8 shows that the stability constant presents the same behavior as in the case of V_n built with transport snapshots.

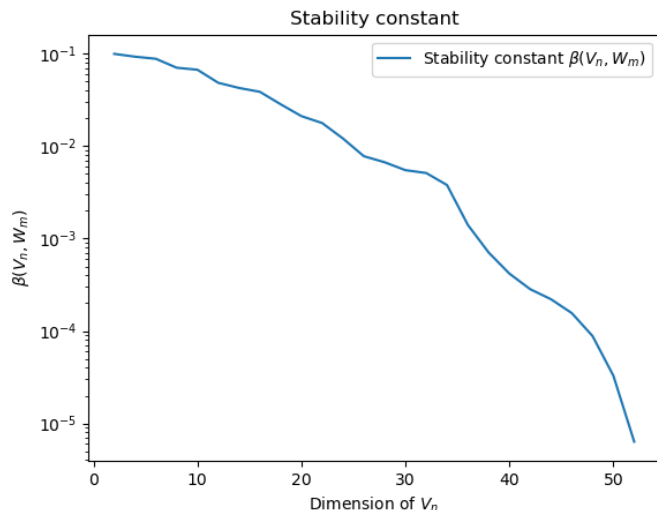


Figure 5: Stability constant $\beta(V_n, W_m)$ with respect to the dimension n of the reduced space

Conclusion of the numerical results and outlook

From the numerical experiments, it follows that the PBDW algorithm can reconstruct data very efficiently when the physical model is perfect. An interesting fact is that there are optimal values n^* for the dimension in the reduced models V_n used in the PBDW algorithm which make the reconstruction with measurement observations be comparable to the approximation accuracy by projection on V_n (see, e.g., Figures 2 and 4).

In presence of model error, the conclusions are analogous. However, the approximation accuracy by direct projection is degraded by the presence of the model error as the comparison between Figure 2 and Figure 6 shows. This degradation may be reduced if some snapshots are computed with the transport model. The selection of these snapshots may be based on a posteriori estimators devised specifically for the model error.

In principle, the PBDW is expected to be able to correct to some extent the model error due to fact that reconstructions lie in $V_n \oplus (W \cap V_n^\perp)$ and not only in V_n . There, if the model is biased and yields a reduced model V_n which is not perfectly appropriate, the component $(W \cap V_n^\perp)$ is expected to help to correct this inaccuracy. However, our results tend to indicate that this correction component has a very limited effect in our case. This may be due to the poor approximation properties of the observation space W , which is, in our case, spanned by functions that are very localized in space (see equation (21) for the definition of the ω_i). This behavior could be improved by working with parametrized families of spaces such as Reproducing Kernel Hilbert spaces (see [34]). In that case, we could try to find an appropriate space for which the ω_i would better enhance the final reconstruction quality. Another option would be to consider

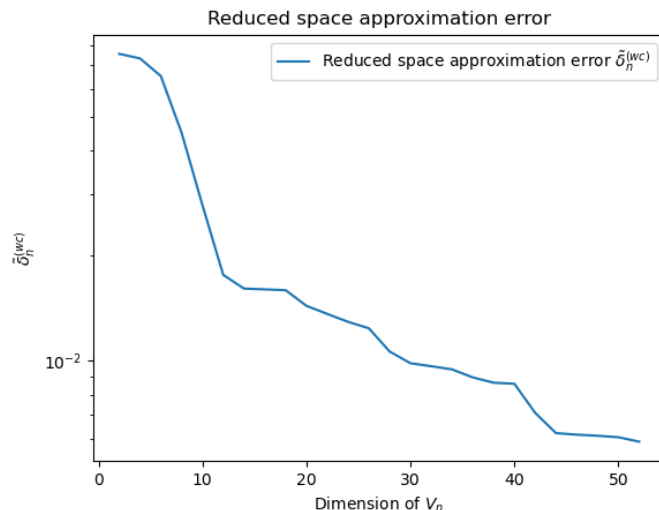


Figure 6: Relative approximation error $\tilde{\delta}_n^{(wc)}$ of the transport manifold \mathcal{M}_{tr} with respect to the dimension n of the reduced space. Here the reduced space is a POD computed using the diffusion manifold $\mathcal{M}_{\text{diff}}$.

purely data-driven corrections on top of the PBDW reconstruction, making use of supervised learning techniques and feed forward neural networks. These ideas will be the starting point of future works in mitigating the effect model error in state estimation.

Acknowledgements

The authors gratefully acknowledge O. Lafitte for fruitful discussions. This project was partly funded by CEA. O.M. was funded by the Emergence project grant of the Paris City Council “Models and Measures”.

References

- [1] Y. Maday, A. T. Patera, J. D. Penn, and M. Yano. A parameterized-background data-weak approach to variational data assimilation: formulation, analysis, and application to acoustics. *International Journal for Numerical Methods in Engineering*, 102(5):933–965, 2015.
- [2] P. Binev, A. Cohen, W. Dahmen, R. DeVore, G. Petrova, and P. Wojtaszczyk. Data assimilation in reduced modeling. *SIAM/ASA Journal on Uncertainty Quantification*, 5(1):1–29, 2017.

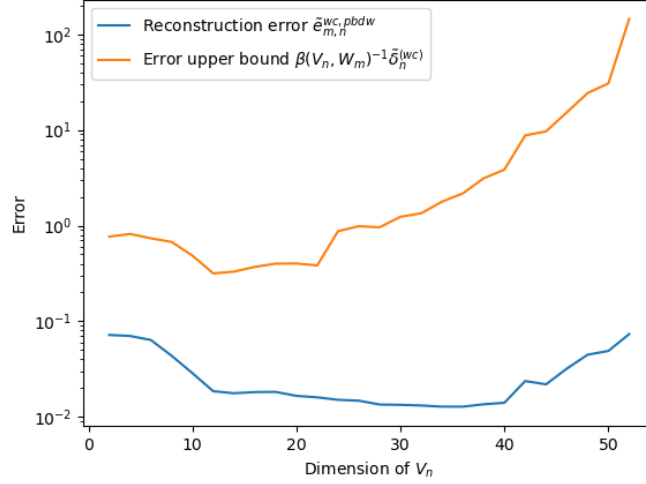


Figure 7: Relative reconstruction error $\tilde{e}_{m,n}^{(wc, pbdw)}$ (in blue) and error estimate $\beta(V_n, W_m)^{-1} \tilde{\delta}_n^{(wc)}$ (in yellow) with respect to the dimension n of the reduced space

- [3] R. DeVore, G. Petrova, and P. Wojtaszczyk. Data assimilation and sampling in banach spaces. *Calcolo*, 54(3):963–1007, 2017.
- [4] A. Cohen, W. Dahmen, R. DeVore, J. Fadili, O. Mula, and J. Nichols. Optimal reduced model algorithms for data-based state estimation. *SIAM Journal on Numerical Analysis*, 58(6):3355–3381, 2020.
- [5] Albert Cohen, Wolfgang Dahmen, Olga Mula, and James Nichols. Nonlinear reduced models for state and parameter estimation. *SIAM/ASA Journal on Uncertainty Quantification*, 10(1):227–267, 2022.
- [6] O. Mula. Inverse problems: A deterministic approach using physics-based reduced models. *Submitted*, 2022.
- [7] J. P. Argaud, B. Bouriquet, H. Gong, Y. Maday, and O. Mula. Stabilization of (g)eim in presence of measurement noise: Application to nuclear reactor physics. In Marco L. Bittencourt, Ney A. Dumont, and Jan S. Hesthaven, editors, *Spectral and High Order Methods for Partial Differential Equations ICOSAHOM 2016: Selected Papers from the ICOSAHOM conference, June 27-July 1, 2016, Rio de Janeiro, Brazil*, pages 133–145, Cham, 2017. Springer International Publishing.
- [8] J. P. Argaud, B. Bouriquet, H. Gong, Y. Maday, and O. Mula. Monitoring flux and power in nuclear reactors with data assimilation and reduced models. In *International Conference*

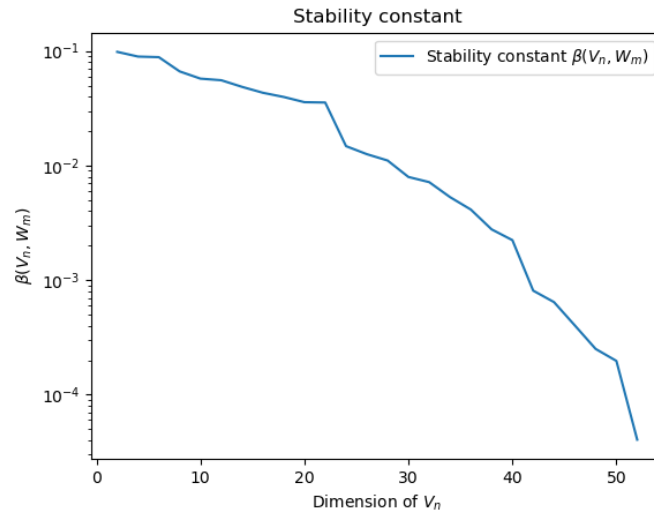


Figure 8: Stability constant $\beta(V_n, W_m)$ with respect to the dimension n of the reduced space

on Mathematics and Computational Methods Applied to Nuclear Science & Engineering. 2017.

- [9] J.-P. Argaud, B. Bouriquet, F. de Caso, H. Gong, Y. Maday, and O. Mula. Sensor placement in nuclear reactors based on the generalized empirical interpolation method. *Journal of Computational Physics*, 363:354 – 370, 2018.
- [10] A. Sartori, A. Cammi, L. Luzzi, and G. Rozza. A reduced basis approach for modeling the movement of nuclear reactor control rods. *Journal of Nuclear Engineering and Radiation Science*, 2(2), 2016.
- [11] H. Gong, W. Chen, C. Zhang, and G. Chen. Fast solution of neutron diffusion problem with movement of control rods. *Annals of Nuclear Energy*, 149:107814, 2020.
- [12] W. Chen, D. Yang, J. Zhang, C. Zhang, H. Gong, B. Xia, B. Quan, and L. Wang. Study of non-intrusive model order reduction of neutron transport problems. *Annals of Nuclear Energy*, 162:108495, 2021.
- [13] P. German and J. C. Ragusa. Reduced-order modeling of parameterized multi-group diffusion k-eigenvalue problems. *Annals of Nuclear Energy*, 134:144–157, 2019.
- [14] S. Lorenzi. An adjoint proper orthogonal decomposition method for a neutronics reduced order model. *Annals of Nuclear Energy*, 114:245–258, 2018.
- [15] A. Hebert. *Applied reactor physics*. Presses inter Polytechnique, 2009.

- [16] T. Taddei. An adaptive parametrized-background data-weak approach to variational data assimilation. *ESAIM: Mathematical Modelling and Numerical Analysis*, 51(5):1827–1858, 2017.
- [17] H. Gong, Y. Maday, O. Mula, and T. Taddei. PBDW method for state estimation: error analysis for noisy data and nonlinear formulation. *arXiv e-prints*, page arXiv:1906.00810, Jun 2019.
- [18] M. Ettehad and S. Foucart. Instances of computational optimal recovery: dealing with observation errors. *SIAM/ASA Journal on Uncertainty Quantification*, 9(4):1438–1456, 2021.
- [19] P. Binev, A. Cohen, W. Dahmen, R. DeVore, G. Petrova, and P. Wojtaszczyk. Data assimilation in reduced modeling. *SIAM/ASA Journal on Uncertainty Quantification*, 5(1):1–29, 2017.
- [20] F. Galarce, J.F. Gerbeau, D. Lombardi, and O. Mula. Fast reconstruction of 3D blood flows from doppler ultrasound images and reduced models. *Computer Methods in Applied Mechanics and Engineering*, 375:113559, 2021.
- [21] A. Cohen and R. DeVore. Approximation of high-dimensional parametric PDEs. *Acta Numerica*, 24:1–159, 2015.
- [22] A. Buffa, Y. Maday, A. T. Patera, C. Prud’homme, and G. Turinici. A priori convergence of the greedy algorithm for the parametrized reduced basis method. *ESAIM: Mathematical Modelling and Numerical Analysis*, 46(3):595–603, 2012.
- [23] G. Rozza, D. B. P. Huynh, and A. T. Patera. Reduced basis approximation and a posteriori error estimation for affinely parametrized elliptic coercive partial differential equations. *Archives of Computational Methods in Engineering*, 15(3):1, Sep 2007.
- [24] A. Cohen, R. DeVore, and C. Schwab. Analytic regularity and polynomial approximation of parametric and stochastic elliptic PDE’s. *Analysis and Applications*, 09(01):11–47, 2011.
- [25] R. Dautray and J.-L. Lions. *Mathematical Analysis and Numerical Methods for Science and Technology: Volume 6 Evolution Problems II*. Springer Science & Business Media, 2012.
- [26] Allaire, G. and Bal, G. Homogenization of the criticality spectral equation in neutron transport. *ESAIM: M2AN*, 33(4):721–746, 1999.
- [27] G. Bal. *Couplage d’équations et homogénéisation en transport neutronique*. PhD thesis, University of Paris 6, France, 1997.

- [28] T. Takeda and H. Ikeda. 3-d neutron transport benchmarks. *Journal of Nuclear Science and Technology*, 28(7):656–669, 1991.
- [29] J.-J. Lautard and J.-Y. Moller. Minaret, a deterministic neutron transport solver for nuclear core calculations. In *Proceedings of M&C 2011*, Rio de Janeiro (Brazil), 2011. American Nuclear Society.
- [30] D. Schneider, F. Dolci, F. Gabriel, J.-M. Palau, M. Guillo, B. Pothet, P. Archier, K. Ammar, F. Auffret, R. Baron, A.-M. Baudron, P. Bellier, L. Bourhrara, L. Buiron, M. Coste-Delclaux, C. De Saint Jean, J.-M. Do, B. Espinosa, E. Jamelot, and I. Zmijarevic. APOLLO3[®] : CEA/DEN deterministic multi-purpose code for reactor physics analysis. In *Proceedings of Physor 2016*, Sun Valley, Idaho (USA), 2016. American Nuclear Society.
- [31] W. H. Reed and T. R. Hill. Triangular mesh methods for the neutron transport equation. Technical Report LA-UR-73-479, Los Alamos National Laboratory, USA, 1973.
- [32] D. A. Di Pietro and A. Ern. *Mathematical aspects of discontinuous Galerkin methods*, volume 69. Springer Science & Business Media, 2011.
- [33] P. Binev, A. Cohen, O. Mula, and J. Nichols. Greedy algorithms for optimal measurements selection in state estimation using reduced models. *SIAM/ASA Journal on Uncertainty Quantification*, 6(3):1101–1126, 2018.
- [34] Yvon Maday and Tommaso Taddei. Adaptive pbdw approach to state estimation: noisy observations; user-defined update spaces. *SIAM Journal on Scientific Computing*, 41(4):B669–B693, 2019.